EUROPEAN ORGANISATION FOR NUCLEAR RESEARCH

A Measurement of τ Polarization in Z^0 Decays

The L3 Collaboration

Abstract

The polarization of τ leptons produced in $e^+e^- \rightarrow \tau^+\tau^-(\gamma)$ is measured using a sample of 8977 $\tau^+\tau^-$ pairs collected near the peak of the Z^0 resonance. A polarization of $-0.132\pm0.026(\text{stat.})\pm0.021(\text{syst.})$ is determined. This corresponds to a ratio of the vector to the axial-vector coupling constants of the τ lepton to the weak neutral current of $(g_V^\tau/g_A^\tau)_{\text{eff}} = 0.069 \pm 0.017$. This leads to a value of the effective $\sin^2 \theta_W$ at the Z^0 resonance of $\sin^2 \theta_{\text{eff}} = 0.2326 \pm 0.0043$.

Introduction

For unpolarized e^+e^- beams, the polarization $\mathcal{P}_f$ of final state fermions in $e^+e^- \to Z^0 \to f^+f^-$ is sensitive to the parity-violating components of the weak neutral current interaction. $\mathcal{P}_f$ is the asymmetry in the total production cross-section σ of positive ($h = +1$) and negative ($h = -1$) helicity fermions

$$\mathcal{P}_f = \frac{\sigma(h = +1) - \sigma(h = -1)}{\sigma(h = +1) + \sigma(h = -1)} \tag{1}$$

If the weak neutral current contains only vector and axial-vector couplings, helicity conservation in the massless limit implies that the initial state e^+e^- and the final state f^+f^- can only involve fermions of opposite helicity; therefore $\mathcal{P}_{f-} = -\mathcal{P}_{f+} \equiv \mathcal{P}_f$.

In the improved Born approximation [1], the polarization at the peak of the Z^0 resonance is given by

$$\mathcal{P}_f \simeq -\frac{2g_V^f g_A^f}{g_V^{f2} + g_A^{f2}} \tag{2}$$

where g_V^f and g_A^f are the effective vector and axial-vector coupling constants of fermion f to the weak neutral current. The average polarization $\mathcal{P}_f$ is thus independent of the coupling constants of the initial state e^+e^-. The measurement of $\mathcal{P}_f$ allows the determination of the relative sign of g_V and g_A, which is not otherwise accessible from observables with unpolarized e^+e^- beams. In the Standard Model [2]

$$\mathcal{P}_l \simeq -2\left(1 - 4\sin^2\theta_W\right) \tag{3}$$

for $l = \mu, \tau$, showing the large sensitivity of $\mathcal{P}_l$ to the effective weak mixing angle $\sin^2\theta_W$, thus making this measurement potentially one of the most precise tests of the Standard Model.

Due to the short decay length of τ leptons and the parity violating V-A structure of the weak charged current decay, $\mathcal{P}_\tau$ can be deduced from an analysis of the kinematics of τ decays [3]. τ leptons of opposite helicity have different decay angular distributions in the τ rest frame, and thus different energy distributions in the laboratory frame. However, in this analysis it is impossible to distinguish the effects of $\mathcal{P}_\tau$ on these decay distributions from those of deviations from the V-A structure of the weak charged current. We assume that no such deviations exist, consistent with existing data on the charged current interaction in τ decays [4, 5]. We study the kinematics of the two body decays $\tau^- \to \pi^-(K^-)\nu_\tau$, $\rho^-\nu_\tau$ and $a_1^-\nu_\tau$ [1] and the three body decays $\tau^- \to e^-\overline{\nu}_e\nu_\tau$ and $\mu^-\overline{\nu}_\mu\nu_\tau$ which together includes 77% of all τ decays.

For the three-body decays, the dependence of the differential cross-section on $\mathcal{P}_\tau$ as a function of $x_l = E_l/E_\tau \simeq E_l/E_{\text{beam}}$ is given to lowest order by [1]

$$\frac{1}{\sigma}\frac{d\sigma}{dx_l} = \frac{1}{3}\left[\left(5 - 9x_l^2 + 4x_l^3\right) + \mathcal{P}_\tau\left(1 - 9x_l^2 + 8x_l^3\right)\right] \tag{4}$$

For the two-body decays, the differential cross-section as a function of $x_h = E_h/E_\tau \simeq E_h/E_{\text{beam}}$ depends linearly on $\mathcal{P}_\tau$ to lowest order [1]

$$\frac{1}{\sigma}\frac{d\sigma}{dx_h} = 1 + \mathcal{P}_\tau\alpha_h\left(2x_h - 1\right) \tag{5}$$

---

[1]In all cases, the decay mode for τ^- is described. The charge conjugate decays are also used in our analysis. The $\tau^- \to \pi^-\nu_\tau$ and $\tau^- \to K^-\nu_\tau$ decay modes are not separated and are combined in the analysis.

1

where α_h is a constant depending on the mass and spin of hadron type h. In the case of $\tau^- \to \pi^-(\mathrm{K}^-)\nu_\tau$, $\alpha_h = 1$. For $\tau^- \to \rho^- \nu_\tau$ and $\mathrm{a}_1^- \nu_\tau$ [6]

$$\alpha_h = \frac{m_\tau^2 - 2m_h^2}{m_\tau^2 + 2m_h^2} \tag{6}$$

where m_h is the mass of the hadron. The sensitivity to $\mathcal{P}_\tau$, which depends on the value of α_h, can be enhanced in the latter case by further analysing the decays of these spin-1 particles [6].

Our data sample corresponds to 410 000 $\mathrm{Z}^0 \to$ hadrons events from an integrated luminosity of 17.6 pb^{-1} collected in 1990 and 1991 on or near the Z^0 peak using the L3 detector at LEP. The center-of-mass energies are distributed over the range $88.2 \le \sqrt{s} \le 94.2$ GeV with 80% of the events collected at $\sqrt{s}$=91.222 GeV [7].

The L3 Detector

The L3 detector includes a central tracking chamber, a high resolution electromagnetic calorimeter, a ring of scintillation counters, a hadron calorimeter and a muon chamber system. All are installed in a large magnet which provides a uniform field of 0.5 Tesla.

The central tracking chamber consists of a time expansion chamber (TEC) surrounded by two thin proportional chambers (Z-Chamber). The TEC is constructed as two coaxial cylindrical drift chambers with 12 inner and 24 outer sectors. The Z-Chamber consists of two coaxial cylindrical multiwire proportional chambers with cathode strip readout. The electromagnetic calorimeter is composed of bismuth germanate (BGO) crystals in the shape of truncated pyramids pointing to the interaction region. The hadron calorimeter uses depleted uranium absorber plates interspersed with proportional wire chambers alternately oriented along and perpendicular to the beam direction. The muon detector consists of three layers of precise drift chambers, measuring the muon trajectory in both the bending and non-bending planes.

The L3 detector and its performance have been described in detail elsewhere [8, 9, 10]. The TEC vertex detector has a momentum resolution of $\sigma(1/P_\mathrm{T}) = 0.022/$GeV and a position resolution at the face of the BGO electromagnetic calorimeter of 0.5 mm in the plane transverse to the beam direction. The Z-chamber has a position resolution of 0.5 mm in the plane parallel to the beam direction. The muon chambers give a momentum resolution of 2.8% for charged particles with $P_\mathrm{T} = 45$ GeV. For this analysis, the longitudinal and transverse development of electromagnetic and hadronic showers in the calorimeters has been calibrated using test beam data for e, μ and $\pi^\pm$'s. The energy resolution of the calorimeters for $\pi^\pm$ is $55\%/\sqrt{E(\mathrm{GeV})}+8\%$ and for e's and γ's is better than 2% above 1.5 GeV.

Event Selection and Particle Identification

The procedures for the selection of electron, muon, pion, rho and a_1 decay modes are designed to be relatively independent of the energy of the τ decay products, in order to minimize the introduction of polarization biases. The preselection removes most of the cosmic ray, two photon and $\mathrm{Z}^0 \to$ hadrons background. This is followed by the identification of electrons and μ's and rejection of $\mathrm{Z}^0 \to \mathrm{e}^+\mathrm{e}^-(\gamma)$ and $\mu^+\mu^-(\gamma)$ events. The final data sample consists of events where at least one of the τ decays into one of the channels listed in the introduction. Selection efficiencies and backgrounds are calculated using Monte Carlo simulation of $\mathrm{Z}^0 \to \tau^+\tau^-(\gamma)$, $\mathrm{e}^+\mathrm{e}^-(\gamma)$, $\mu^+\mu^-(\gamma)$, $\mathrm{Z}^0 \to$ hadrons, and two photon reactions [11, 12] including full simulation

2

Channel	Number Decays 1990	Number Decays 1991
$e^-\overline{\nu}_e\nu_\tau$	385	2016
$\mu^-\overline{\nu}_\mu\nu_\tau$	558	1844
$\pi^-(K^-)\nu_\tau$	220	1603
$\rho^-\nu_\tau$	503	3130
a_1	-	473

Table 1: Summary of the number of decays for each channel. The $\tau^- \to a_1^-\nu_\tau$ channel was not analysed in 1990.

of the L3 detector response [13]. The same selection criteria are applied to data and Monte Carlo events and the number of selected decays for each channel is listed in Table 1.

Preselection

Cosmic ray events are reduced to negligible levels by using scintillator time-of-flight information for muon chamber tracks and requiring at least one TEC track to pass within 5 mm of the interaction region. Each event is required to have at least one TEC track with an associated Z-chamber hit, confining the selection to the fiducial volume $42^o < \theta < 138^o$ (θ is the measured from the electron beam axis) covered by the barrel BGO calorimeter. The two photon background is suppressed by requiring at least one track to have a transverse momentum greater than 0.5 GeV and by rejecting events where the vector sum of the transverse momenta of the tracks is less than 4 GeV and the total calorimetric energy is less than 15 GeV.

To remove $Z^0 \to$ hadrons, events with more than six tracks are rejected. The thrust axis of each remaining event is calculated using calorimeter and muon chamber information. The plane perpendicular to the thrust axis through the interaction vertex defines two hemispheres for each event. Neither hemisphere in an event can contain more than five tracks. Events where one of the tracks makes an angle greater than 20° with the thrust axis in the plane transverse to the beam are rejected, taking advantage of the high boost and low invariant mass of each jet in dilepton events compared with $Z^0 \to$ hadrons events. The number of clusters in the BGO calorimeter is required to be less than 20. These cuts reject more than 99.9% of $Z^0 \to$ hadrons events while rejecting less than 2% of the dilepton events.

The data sample now consists of 34203 events which includes more than 98% of each of the charged leptonic Z^0 decay modes and a background of 5% mainly from two photon interactions and $Z^0 \to$ hadrons. For the one-prong channels described below, each hemisphere with exactly one track and an associated Z-chamber hit is considered for selection.

Selection of $\tau^- \to e^-\overline{\nu}_e\nu_\tau$

The identification of electrons requires the shower shape in the BGO calorimeter to be symmetric and narrow, characteristic of an electromagnetic shower. To reject hadronic decays with $\pi^\pm$'s merged a π^0, the angle between the track and the nearest BGO cluster is required to be less than 25 mrad and 40 mrad in the planes perpendicular and parallel to the beam direction respectively. Hemispheres with hadronic or minimum ionizing showers in the hadron calorimeter or tracks in the muon chambers are rejected.

To remove $Z^0 \to e^+e^-(\gamma)$ events, events with two identified electrons are rejected; the total

energy deposited in the BGO calorimeter is required to be less than 85% of the center of mass energy and the shower development of the jet in the recoil hemisphere has to be compatible with that expected for $\pi^\pm$ or μ's. To reject misidentified μ's with overlapping γ's and $\pi^\pm$'s with completely overlapping π^0's, the energy measured in the BGO calorimeter is combined with the momentum measured in the TEC by maximising the likelihood for the two measurements to originate from a single electron. The likelihood which measures the compatibility of this average is required to be less than 8.

The selection efficiency is estimated to be 76% in 1991 and 32% in 1990 [2] inside the fiducial region and is independent of electron energy above 8 GeV. The backgrounds are 2.9% from other τ decays, 4.1% from $Z^0 \rightarrow e^+ e^- (\gamma)$, 0.3% from $Z^0 \rightarrow \mu^+ \mu^- (\gamma)$ and 0.3% from two photon interactions.

Selection of $\tau^- \rightarrow \mu^- \overline{\nu}_\mu \nu_\tau$

Hemispheres with one reconstructed muon chamber track consisting of hits from at least two layers of muon chambers are considered for selection. This track is required to originate from within 50 cm of the interaction region both transverse and perpendicular to the beam direction. The shower development in the calorimeters is required to be consistent with that expected from a minimum ionizing particle with at most one additional electromagnetic shower.

$Z^0 \rightarrow \mu^+ \mu^- (\gamma)$ events are removed by excluding events with two identified μ's as well as those in which the recoil hemisphere contains either a shower profile compatible with a minimum ionizing particle or a muon chamber track with momentum greater than 20 GeV. To reject $\pi^\pm$'s, the difference in the inverse transverse momentum measured in the muon chambers and in the TEC is required to be within 3.5 times the error in this quantity.

The selection efficiency is estimated to be 72% inside the fiducial region and is independent of the muon momentum above 8 GeV. The background contributions are 1.4% from other τ decays and 2.5% from $Z^0 \rightarrow \mu^+ \mu^- (\gamma)$ and two photon reactions.

Selection of $\tau^- \rightarrow \pi^- (K^-) \nu_\tau$ and $\rho^- \nu_\tau$

For the selection of $\tau^- \rightarrow \pi^- (K^-) \nu_\tau$ and $\rho^- \nu_\tau$, the preselection and dilepton rejection described above are imposed and hemispheres which contain identified electrons and μ's are rejected. The data sample then consists mainly of $\tau^- \rightarrow \pi^- (K^-) \nu_\tau$, $\rho^- \nu_\tau$ and one-prong $a_1^- \nu_\tau$ decays. To facilitate discrimination between these decays, an algorithm for finding neutral clusters in the BGO calorimeter is used, with the emphasis on finding π^0 showers overlapped with charged particle showers.

First the energy profile of the charged pion shower in the BGO calorimeter is estimated, normalizing to the energy deposited in the BGO crystal impacted by the TEC track (central crystal). The energy profile in the BGO calorimeter, which is determined from the test beam study, is relatively independent of the incident charged pion energy. The energy determined from the normalized profile is subtracted from each crystal in a $30°$ half angle cone surrounding the central crystal and a search is made for secondary clusters. Clusters formed inside a cone of half angle 25 mrad around the track are ignored. The energy profiles of any neutral clusters found are estimated assuming they originated from π^0's and a better estimate of the energy

---

[2]The selection efficiency in the electron, $\rho^\pm$ and $\pi^\pm$ channels is lower for the 1990 data due to a lower Z-chamber effeciency during the 1990 run.

deposited in the central crystal is obtained. This procedure is iterated until all reconstructed particle energies are stable to 1%, typically after three to four iterations.

$\tau^- \rightarrow \pi^-(K^-)\nu_\tau$ decays typically contain low energy neutral clusters arising from fluctuations in the charged pion shower profile while the π^0's in $\tau^- \rightarrow \rho^-\nu_\tau$ and $a_1^-\nu_\tau$ decays give rise to higher energy neutral clusters whose shower developments are electromagnetic in shape. Two neutral clusters are considered to form a π^0 candidate if their invariant mass is within 35 MeV of the π^0 mass. A single neutral cluster forms a π^0 candidate if its energy exceeds 3 GeV and its transverse profile is consistent with being purely electromagnetic.

Hemispheres containing π^0 candidates outside a cone of half angle 40 mrad around the track are rejected in the $\tau^- \rightarrow \pi^-(K^-)\nu_\tau$ selection. To select the final sample of these decays, the momentum of the track is required to exceed 5% of the beam energy, due to the poor separation between electron, μ and $\pi^\pm$'s below this energy. The energies of the most energetic and second most energetic neutral clusters are required to be less than 4 GeV and 1 GeV respectively. To further reduce background where the $\pi^\pm$ and π^0 are unresolved, the total BGO energy transverse to the track is required to be less than 0.4 GeV, taking advantage of the higher invariant mass of $\tau^- \rightarrow \rho^-\nu_\tau$ decays. As in the electron selection, the likelihood formed after averaging the energy measured in the calorimeters and the corresponding TEC momentum is required to be less than 2.5.

The selection efficiency in the fiducial volume is 63% for 1991 (Fig. 1) and 27% in 1990. The background is 12%, 2.3% and 0.5% from other τ decays, $Z^0 \rightarrow \mu^+\mu^-(\gamma)$ and two photon events respectively.

To select the final sample of $\tau^- \rightarrow \rho^-\nu_\tau$ decays, exactly one π^0 candidate is required in the hemisphere. Hemispheres with additional neutral clusters compatible with being electromagnetic are rejected. The estimated energy deposited by the π^0 candidate is subtracted from the total calorimetric energy and the remainder is assigned to the $\pi^\pm$. The likelihood for the combined $\pi^\pm$ energy and the TEC momentum measurement of the $\pi^\pm$ is required to be less than 4.

Fig. 2a shows the $\pi^\pm\pi^0$ invariant mass for these selected decays. The mass resolution varies between 30 MeV and 120 MeV. A fit to the distribution using a phase-space-suppressed Breit-Wigner resonance formula [6] convolved with the detector resolution yields $M_\rho = 772 \pm 7(\text{stat.}) \pm 20(\text{syst.})$ MeV and $\Gamma_\rho = 163 \pm 11(\text{stat.}) \pm 9(\text{syst.})$ MeV, consistent with the current world averages [14] for M_ρ and Γ_ρ. The selection efficiency in the fiducial volume is 64% in 1991 and 30% in 1990. The background is 17% from other τ decays and 1% from two photon interactions and other sources.

The pion energies $E_{\pi\pm}$ and E_{π^0} and momenta $\mathbf{p}_{\pi\pm}$ and $\mathbf{p}_{\pi^0}$ are related to the decay angles θ^*, the angle in the τ rest frame between the $\rho^\pm$ and the τ line of flight, and ψ^*, the angle in the $\rho^\pm$ rest frame between the $\pi^\pm$ and $\rho^\pm$ line of flight, by [6]

$$\cos\theta^* = \frac{4m_\tau^2}{m_\tau^2 - m_\rho^2} \frac{E_{\pi^0} + E_{\pi\pm}}{\sqrt{s}} - \frac{m_\tau^2 + m_\rho^2}{m_\tau^2 - m_\rho^2}$$

and

$$\cos\psi^* = \frac{m_\rho}{\sqrt{m_\rho^2 - 4m_\pi^2}} \frac{E_{\pi\pm} - E_{\pi^0}}{|\mathbf{p}_{\pi\pm} + \mathbf{p}_{\pi^0}|}$$

Figs. 2b and 2c respectively show the efficiency for $\tau^- \rightarrow \rho^-\nu_\tau$ events as a function of $\cos\theta^*$ and $\cos\psi^*$.

5

Selection of $\tau^- \to a_1^- \nu_\tau$

$\tau^- \to a_1^- \nu_\tau$ decays are selected from the data sample after preselection by searching for the decay of the a_1 into three $\pi^\pm$'s. Candidate events are those containing three TEC tracks in one hemisphere. The acollinearity of the event is required to be less than 30° in order to reject two photon events.

The decay $a_1^- \to \pi^+\pi^-\pi^-$ is known [14] to proceed dominantly through the intermediate state $\rho^0\pi^-$. There are two combinations of the three $\pi^\pm$'s which can contribute to this process and the corresponding amplitudes must be added [15]. We take advantage of this by requiring that at least one of the two pairs of oppositely charged $\pi^\pm$'s form a system of invariant mass greater than 0.5 GeV. The dominant remaining background is that from the process $\tau^- \to \pi^-\pi^+\pi^- + n\pi^0$; we require that the total energy deposited in the BGO calorimeter in the hemisphere be less than 8 GeV.

A fit is performed to combine the total calorimetric energy with the total momentum measured with the TEC to give the best estimate of the $\pi^\pm$ momenta. The $\pi^\pm$ momenta are then used to determine the quantities $\cos\theta$, the cosine of angle between the momentum of the three $\pi^\pm$ system and the τ direction of flight as determined in the rest frame of the τ, and $\cos\psi$, the angle between the normal to the plane spanned by the three $\pi^\pm$ in their rest frame and the momentum of the three $\pi^\pm$ system. Since the normal to the plane is determined only up to a sign, only the absolute value of $\cos\psi$ is physically significant. Estimates c_θ (c_ψ) of $\cos\theta$ ($|\cos\psi|$) are determined from the measured $\pi^\pm$'s momenta using analytic approximations [16]

$$c_\theta = \frac{4m_\tau^2}{m_\tau^2 - m^2} \frac{(E_1 + E_2 + E_3)}{\sqrt{s}} - \frac{m_\tau^2 + m^2}{m_\tau^2 - m^2}$$

$$c_\psi = \frac{8m^2 |\mathbf{p}_1 \cdot (\mathbf{p}_2 \times \mathbf{p}_3)| / |\mathbf{p}_1 + \mathbf{p}_2 + \mathbf{p}_3|}{\sqrt{-\lambda(\lambda(m^2, m_{12}^2, m_\pi^2), \lambda(m^2, m_{13}^2, m_\pi^2), \lambda(m^2, m_{23}^2, m_\pi^2))}}$$

$$\lambda(x, y, z) = x^2 + y^2 + z^2 - 2xy - 2yz - 2zx$$

where p_i is the three momentum of $\pi^\pm$ i, m_{ij} is the invariant mass of $\pi^\pm$'s i and j, and m is the invariant mass of the three $\pi^\pm$ system. Events whose measured momenta are inconsistent with a_1 decay kinematics are rejected.

The observed invariant mass distribution of the selected a_1 candidates is shown together with the expected distribution from Monte Carlo events [12] in Fig. 3. The mass determined by the fit [15] is 1.186 ± 0.060 GeV, which is consistent with the Particle Data Group value [14] and also agrees with more recent measurements [17].

The selection efficiency is estimated to be 37% for 1991 in the fiducial volume and the background is estimated to be 11%, mainly from $\tau^- \to \pi^-\pi^+\pi^- + n\pi^0$.

Measurement of $\mathcal{P}_\tau$

For each τ decay channel, $\mathcal{P}_\tau$ is measured by obtaining the linear combination of the $h = +1$ and $h = -1$ Monte Carlo distributions which best fits the data. For $\tau^- \to e^-\overline{\nu}_e\nu_\tau$, $\mu^-\overline{\nu}_\mu\nu_\tau$ and $\pi^-(K^-)\nu_\tau$, the energy distribution of the charged particle is used and the overall normalization and polarization are left as free parameters in a binned maximum likelihood fit. For $\tau^- \to \rho^-\nu_\tau$ and $a_1^-\nu_\tau$, multidimensional distributions are used as described below. For each decay mode, the polarization of the background from other τ decays is varied simultaneously with

Channel	Selection	Background	Calibration	Radiative Corrections	Monte Carlo Statistics
$e^-\overline{\nu}_e\nu_\tau$	0.027	0.020	0.020	0.020	0.046
$\mu^-\overline{\nu}_\mu\nu_\tau$	0.020	0.020	0.020	0.010	0.046
$\pi^-(K^-)\nu_\tau$	0.017	0.009	0.013	0.005	0.021
$\rho^-\nu_\tau$	0.013	0.005	0.020	negl.	0.016
a_1	0.045	0.010	0.033	negl.	0.073

Table 2: Summary of systematic errors for all channels

Channel	$\mathcal{P}_\tau$	Stat. Error	Syst. Error
$e^-\overline{\nu}_e\nu_\tau$	-0.127	0.097	0.062
$\mu^-\overline{\nu}_\mu\nu_\tau$	-0.020	0.101	0.055
$\pi^-(K^-)\nu_\tau$	-0.148	0.046	0.033
$\rho^-\nu_\tau$	-0.152	0.035	0.029
a_1	0.105	0.164	0.093

Table 3: Summary for $\mathcal{P}_\tau$ and errors for all channels

the polarization for the decay mode being fit. The statistical error in each channel is verified by direct calculation from the functional form of the decay distributions after including the kinematics, efficiency corrections and detector resolution. The statistical errors due to limited Monte Carlo statistics are included in the calculation of the systematic errors. A breakdown of systematic errors for each channel is given in Table 2 and the result for each channel is given in Table 3.

$\tau^- \rightarrow e^-\overline{\nu}_e\nu_\tau$

The sum of the energies in the three most energetic BGO clusters in the hemisphere, assuming they originated from electrons and γ's, is used to estimate the energy of electron candidates.

Background for $Z^0 \rightarrow e^+e^-(\gamma)$ is determined by selecting dielectron data events which pass the all the $\tau^- \rightarrow e^-\overline{\nu}_e\nu_\tau$ cuts except the cuts which reject events with identified electrons in each hemisphere and events with BGO calorimeter energy greater than 85% of the center of mass energy. A three parameter fit to the data and all backgrounds is first performed in the range $0.0 < E_{\text{BGO}}/E_{\text{beam}} < 1.1$ with the normalization of dielectron background as a free parameter. The dielectron background is then fixed to the fit value and a two parameter fit is performed in the range $0.0 < E_{\text{BGO}}/E_{\text{beam}} < 0.95$ to determine the polarization and overall normalization. The small background from two photon events is determined by Monte Carlo.

The systematic error from $Z^0 \rightarrow e^+e^-(\gamma)$ background subtraction is estimated by varying its normalization by the statistical error extracted from the three parameter fit. The systematic errors from variations in the background from other τ decays are small. The accuracy of the BGO energy scale is known within 2% at 1 GeV by a study of test beam data and $e^+e^- \rightarrow e^+e^-e^+e^-$ events in the data and 0.3% at 45 GeV from $Z^0 \rightarrow e^+e^-(\gamma)$ events in the data.

The result for $\tau^- \rightarrow e^-\overline{\nu}_e\nu_\tau$ is $\mathcal{P}_\tau = -0.127 \pm 0.097 \pm 0.062$ where the first error is statistical and the second is systematic. The electron energy spectrum together with the best fit Monte Carlo spectrum are shown in Fig. 4.

7

$$\tau^- \rightarrow \mu^- \overline{\nu}_\mu \nu_\tau$$

The momentum measured in the muon chambers is combined with the most probable energy loss in the calorimeters to estimate the energy of muon candidates. A three parameter fit is first performed in the range $0.05 < E_\mu/E_{\mathrm{beam}} < 1.1$ with the normalization of the $Z^0 \rightarrow \mu^+\mu^-(\gamma)$ background as an additional parameter. The background normalization is then fixed to the fitted value and a two parameter fit performed in the range $0.05 < E_\mu/E_{\mathrm{beam}} < 0.95$. All other backgrounds are determined by Monte Carlo.

The systematic error from the $Z^0 \rightarrow \mu^+\mu^-(\gamma)$ background is estimated by varying its normalization by the statistical error extracted from the three parameter fit. The systematic errors from variations in the background from other τ decays are small. The accuracy of the muon momentum scale is estimated to be 0.2% at 45 GeV. At lower momenta, the absolute muon momentum scale is dominated by the muon energy loss in the calorimeters which is known to within 100 MeV. The ratio of the number of μ's which have hits in three of the muon chambers to the number which have hits in two chambers was checked to ensure that the energy dependence of the efficiency is well understood and the polarization bias from this source is negligible.

The result for $\tau^- \rightarrow \mu^- \overline{\nu}_\mu \nu_\tau$ is $\mathcal{P}_\tau = -0.020 \pm 0.101 \pm 0.055$. The muon momentum spectrum together with the best fit Monte Carlo spectrum are shown in Fig. 5.

$$\tau^- \rightarrow \pi^-(\mathrm{K}^-)\nu_\tau$$

The energies deposited in the calorimeters are used to estimate the energy of the $\pi^\pm$ using the test beam calibration. This energy is combined with the momentum in the TEC to measure the most likely value of the energy assuming the presence of a single $\pi^\pm$.

The absolute energy scales of the BGO and hadron calorimeters are known within 2% each from the comparison of data and Monte Carlo energy spectra normalized to the TEC momentum for $\tau^- \rightarrow \pi^-(\mathrm{K}^-)\nu_\tau$. The $\rho^\pm$ invariant mass from $\tau^- \rightarrow \rho^-\nu_\tau$ also shows that the shift in energy scale is less than 2% in each of the two calorimeters. The accuracy of the momentum scale in the TEC for momenta below 10 GeV is determined to be 2% by a study of the invariant mass of $\mathrm{K_S} \rightarrow \pi^+\pi^-$ in $Z^0 \rightarrow$ hadrons events and from a comparison of the momenta measured in the TEC and the muon chambers in $\tau^- \rightarrow \mu^- \overline{\nu}_\mu \nu_\tau$ decays. The systematic error due to possible differences in the data and Monte Carlo $\pi^\pm$ energy resolution is estimated by a comparison of the resolution derived independently from test beam data and Monte Carlo simulation. From this study, the $\pi^\pm$ energy resolution is parametrized as $\sigma_E/E = (55 \pm 5)\%/\sqrt{E(\mathrm{GeV})} + (8 \pm 1)\%$ and the uncertainty in the energy resolution is included in the systematic error.

The systematic uncertainty due to the background to $\tau^- \rightarrow \pi^-(\mathrm{K}^-)\nu_\tau$ is determined by varying the fraction of $\tau^- \rightarrow \rho^-\nu_\tau$, $\tau^- \rightarrow \mathrm{K}^{*\pm}\nu_\tau$ and $Z^0 \rightarrow \mu^+\mu^-(\gamma)$ decays by 10%, 20% and 30% respectively, accounting for statistical and systematic uncertainties in the estimation of these backgrounds in the Monte Carlo.

The result for $\tau^- \rightarrow \pi^-(\mathrm{K}^-)\nu_\tau$ is $\mathcal{P}_\tau = -0.148 \pm 0.046 \pm 0.033$. The $\pi^\pm$ energy spectrum together with the best fit Monte Carlo spectrum are shown in Fig. 6.

$$\tau^- \rightarrow \rho^- \nu_\tau$$

$\mathcal{P}_\tau$ is determined from a two dimensional fit of $\cos \theta^*$ and $\cos \psi^*$ [6]. To take advantage of the variation of the sensitivity of $\mathcal{P}_\tau$ as a function of the $\rho^\pm$ invariant mass, the sample is divided into nine 100 MeV mass intervals from 0.35 GeV to 1.25 GeV and fit separately in each interval.

$\mathcal{P}_\tau$ is obtained by maximising the likelihood function in a 20×20 matrix in the parameter space of $\cos \theta^*$ and $\cos \psi^*$ taking into account statistical errors in both the data and the Monte Carlo distributions. Owing to the large number of bins, we derive the probability for finding n data events in a bin given n' Monte Carlo events in the same bin for a Monte Carlo sample six times larger than the data sample assuming both the data and Monte Carlo follow a Poisson distribution. This probability is then used in a binned likelihood fit to determine $\mathcal{P}_\tau$.

Systematic errors due to the accuracy of the charged pion energy scale and due to background uncertainties are estimated using a procedure analogous to that used for the $\tau^- \to \pi^-(K^-)\nu_\tau$ channel. In addition, the estimated accuracy of 1% in the energy scale of the π^0 is taken into account. The systematic error from uncertainties in the $\pi^\pm$ shower profile is estimated by a comparison of the opening angle between the $\pi^\pm$ and the π^0 in the data and in the Monte Carlo as a function of the difference in their energies in the BGO calorimeter. The bias of the central value of the fit due to limited Monte Carlo statistics is studied by fitting the data and Monte Carlo distributions to analytical formulae [16] and found to be negligible.

The fit yields $\mathcal{P}_\tau = -0.152 \pm 0.035 \pm 0.029$. Distributions of $\cos \psi^*$ together with the best fit Monte Carlo distributions are shown in Fig. 7 for four different ranges in $\cos \theta^*$.

As a cross check, a method using a neural network technique is applied to select the decays $\tau^- \to \rho^- \nu_\tau$ [18] with an efficiency of 54% in the fiducial volume. Since the selection is based on global energy/cluster distributions which cannot distinguish $\pi^\pm$ and π^0 in the BGO calorimeter, we can only measure the total energy of the $\rho^\pm$ (E_ρ) and the momentum of the $\pi^\pm$ ($P_{\pi\pm}$). The energy of the π^0 is then $E_{\pi^0} = E_\rho - P_{\pi\pm}$. Using a binned maximum likelihood fit to a two dimensional distribution of $\cos \theta^*$ and $\cos \psi^*$ with 20 bins of each variable, we obtain a polarization of $P_\tau = -0.129 \pm 0.050 \pm 0.050$ which is consistent with the result above.

$\tau^- \to a_1^- \nu_\tau$

The polarization in the $\tau^- \to a_1^- \nu_\tau$ channel is determined by a two dimensional fit with 20 bins in c_θ and 10 bins in c_ψ. In a manner similar to that used for the $\rho^\pm$ channel, a fit is performed taking care to account for the effects of limited Monte Carlo statistics in the likelihood function. The fit, performed for 473 decays with a three $\pi^\pm$ invariant mass less than 1.6 GeV, yields a result of $P_\tau = 0.105 \pm 0.164 \pm 0.093$.

Conclusions

The final results for each decay channel are summarized in Table 3. The weighted mean of all five decay modes is
$$\mathcal{P}_\tau = -0.132 \pm 0.026(\text{stat.}) \pm 0.021(\text{syst.}) \qquad (7)$$
This value has smaller errors than previously published measurements [19]. In calculating the average, statistical correlations in events where both hemispheres are used, as well as systematic correlations in the energy calibration of $\pi^\pm$'s in the $\pi^-(K^-)\nu_\tau$, $\rho^- \nu_\tau$ and $a_1^- \nu_\tau$ channels are taken into account. All other systematic errors are assumed to be uncorrelated and are added in quadrature.

Our measurement of $\mathcal{P}_\tau$ implies that parity is violated in the neutral current process $Z^0 \to \tau^+ \tau^- (\gamma)$, as has been previously found in other neutral current processes [20].

Using the above value for $\mathcal{P}_\tau$ and applying a correction of 0.002 to account for initial state

radiation and data collected off the Z^0 resonance, we obtain

$$(\frac{g_V^\tau}{g_A^\tau})_{\text{eff}} = 0.069 \pm 0.017 \tag{8}$$

This can be used to extract the effective weak mixing angle at the Z^0 resonance [21]

$$\sin^2 \theta_{\text{eff}} = 0.2326 \pm 0.0043 \tag{9}$$

This is consistent with other L3 measurements of the weak mixing angle from the study of the Z^0 lineshape and the forward backward asymmetries in the processes $Z^0 \rightarrow b\bar{b}$, $Z^0 \rightarrow e^+e^-(\gamma)$, $Z^0 \rightarrow \mu^+\mu^-(\gamma)$ and $Z^0 \rightarrow \tau^+\tau^-(\gamma)$ [7].

Acknowledgments

10

The L3 Collaboration:

O.Adriani[14] M.Aguilar-Benitez[23] S.Ahlen[9] H.Akbari[5] J.Alcaraz[15] A.Aloisio[26] G.Alverson[10] M.G.Alviggi[26] G.Ambrosi[31] Q.An[16] H.Anderhub[44] A.L.Anderson[13] V.P.Andreev[35] T.Angelov[13] L.Antonov[39] D.Antreasyan[7] P.Arce[23] A.Arefiev[25] A.Atamanchuk[35] T.Azemoon[3] T.Aziz[8,1] P.V.K.S.Baba[16] P.Bagnaia[34] J.A.Bakken[33] L.Baksay[40] R.C.Ball[3] S.Banerjee[8] J.Bao[5] R.Barillère[15] L.Barone[34] A.Baschirotto[24] R.Battiston[31] A.Bay[17] F.Becattini[14] U.Becker[13,44] F.Behner[44] J.Behrens[44] S.Beingessner[4] Gy.L.Bencze[11] J.Berdugo[23] P.Berges[13] B.Bertucci[31] B.L.Betev[39,44] M.Biasini[31] A.Biland[44] G.M.Bilei[31] R.Bizzarri[34] J.J.Blaising[4] G.J.Bobbink[15,2] M.Bocciolini[14] R.Bock[1] A.Böhm[1] B.Borgia[34] M.Boseti[24] D.Bourilkov[28] M.Bourquin[17] D.Boutigny[4] B.Bouwens[2] E.Brambilla[26] J.G.Branson[36] I.C.Brock[32] M.Brooks[21] C.Buisson[22] A.Bujak[41] J.D.Burger[13] W.J.Burger[17] J.P.Burq[22] J.Busenitz[40] X.D.Cai[16] M.Capell[20] M.Caria[31] G.Carlino[26] F.Carminati[14] A.M.Cartacci[14] R.Castello[24] M.Cerrada[23] F.Cesaroni[34] Y.H.Chang[13] U.K.Chaturvedi[16] M.Chemarin[22] A.Chen[47] C.Chen[6] G.M.Chen[6] H.F.Chen[18] H.S.Chen[6] J.Chen[13] M.Chen[13] M.L.Chen[3] W.Y.Chen[16] G.Chiefari[26] C.Y.Chien[5] M.Chmeissani[3] M.T.Choi[46] S.Chung[13] C.Civinini[14] I.Clare[13] R.Clare[13] T.E.Coan[21] H.O.Cohn[29] G.Coignet[4] N.Colino[15] A.Contin[7] F.Crijns[28] X.T.Cui[16] X.Y.Cui[16] T.S.Dai[13] R.D'Alessandro[14] R.de Asmundis[26] A.Degré[4] K.Deiters[13] E.Dénes[11] P.Denes[33] F.DeNotaristefani[34] M.Dhina[44] D.DiBitonto[40] M.Diemoz[34] H.R.Dimitrov[39] C.Dionisi[34,15] M.T.Dova[16] E.Drago[26] T.Driever[28] D.Duchesneau[17] P.Duinker[2] I.Duran[37] S.Easo[31] H.El Mamouni[22] A.Engler[32] F.J.Eppling[13] F.C.Erné[2] P.Extermann[17] R.Fabbretti[42] M.Fabre[42] S.Falciano[34] S.J.Fan[38] O.Fackler[20] J.Fay[22] M.Felcini[15] T.Ferguson[32] D.Fernandez[23] G.Fernandez[23] F.Ferroni[34] H.Fesefeldt[1] E.Fiandrini[31] J.Field[17] F.Filthaut[28] G.Finocchiaro[34] P.H.Fisher[5] G.Forconi[17] T.Foreman[2] K.Freudenreich[44] W.Friebel[43] M.Fukushima[13] M.Gailloud[19] Yu.Galaktionov[25,13] E.Gallo[14] S.N.Ganguli[8] P.Garcia-Abia[23] S.S.Gau[47] D.Gele[22] S.Gentile[34,15] S.Goldfarb[10] Z.F.Gong[18] E.Gonzalez[23] P.Göttlicher[1] D.Goujon[17] G.Gratta[30] C.Grinnell[13] M.Gruenewald[30] C.Gu[16] M.Guanziroli[16] J.K.Guo[38] V.K.Gupta[33] A.Gurtu[15,8] H.R.Gustafson[3] L.J.Gutay[41] K.Hangarter[1] A.Hasan[16] D.Hauschildt[2] C.F.He[38] T.Hebbeker[1] M.Hebert[36] G.Herten[13] U.Herten[1] A.Hervé[15] K.Hilgers[1] H.Hofer[44] H.Hoorani[17] G.Hu[16] G.Q.Hu[38] B.Ille[22] M.M.Ilyas[16] V.Innocente[15,26] H.Janssen[15] S. Jezequel[4] B.N.Jin[6] L.W.Jones[3] A.Kasser[19] R.A.Khan[16] Yu.Kamyshkov[29] P.Kapinos[35,43] J.S.Kapustinsky[21] Y.Karyotakis[15,4] M.Kaur[16] S.Khokhar[16] M.N.Kienzle-Focacci[17] J.K.Kim[46] S.C.Kim[46] Y.G.Kim[46] W.W.Kinnison[21] D.Kirkby[30] S.Kirsch[43] W.Kittel[28] A.Klimentov[13,25] A.C.König[28] E.Koffeman[2] O.Kornadt[1] V.Koutsenko[13,25] A.Koulbardis[35] R.W.Kraemer[32] T.Kramer[13] V.R.Krastev[39,31] W.Krenz[1] A.Krivshich[35] H.Kuijten[28] K.S.Kumar[12] A.Kunin[12,25] G.Landi[14] D.Lanske[1] S.Lanzano[26] P.Lebrun[22] P.Lecomte[44] P.Lecoq[15] P.Le Coultre[44] D.M.Lee[21] I.Leedom[10] J.M.Le Goff[15] R.Leiste[43] M.Lenti[14] E.Leonardi[34] J.Lettry[44] X.Leytens[2] C.Li[18,16] H.T.Li[6] P.J.Li[38] X.G.Li[6] J.Y.Liao[38] W.T.Lin[47] Z.Y.Lin[18] F.L.Linde[15,2] B.Lindemann[1] D.Linnhofer[44] L.Lista[26] Y.Liu[16] W.Lohmann[43,15] E.Longo[34] Y.S.Lu[6] J.M.Lubbers[15] K.Lübelsmeyer[1] C.Luci[34] D.Luckey[7,13] L.Ludovici[34] L.Luminari[34] W.Lustermann[43] J.M.Ma[6] W.G.Ma[18] M.MacDermott[44] P.K.Malhotra[8,†] R.Malik[16] A.Malinin[4,25] C.Maña[23] D.N.Mao[3] Y.F.Mao[6] M.Maolinbay[44] P.Marchesini[44] F.Marion[4] A.Marin[9] J.P.Martin[22] L.Martinez-Laso[23] F.Marzano[34] G.G.G.Massaro[2] T.Matsuda[13] K.Mazumdar[8] P.McBride[12] T.McMahon[41] D.McNally[44] Th.Meinholz[1] M.Merk[28] L.Merola[26] M.Meschini[14] W.J.Metzger[28] Y.Mi[19] G.B.Mills[21] Y.Mir[16] G.Mirabelli[34] J.Mnich[1] M.Möller[1] B.Monteleoni[14] R.Morand[4] S.Morganti[34] N.E.Moulai[16] R.Mount[30] S.Müller[1] A.Nadtochy[35] E.Nagy[11] M.Napolitano[26] H.Newman[30] C.Neyer[44] M.A.Niaz[16] A.Nippe[1] H.Nowak[43] G.Organtini[34] D.Pandoulas[1] S.Paoletti[14] P.Paolucci[26] G.Passaleva[14,31] S.Patricelli[26] T.Paul[5] M.Pauluzzi[31] F.Pauss[44] Y.J.Pei[1] S.Pensotti[24] D.Perret-Gallix[4] J.Perrier[17] A.Pevsner[5] D.Piccolo[26] M.Pieri[15,14] P.A.Piroué[33] F.Plasil[29] V.Plyaskin[25] M.Pohl[44] V.Pojidaev[25,14] N.Produit[17] J.M.Qian[3] K.N.Qureshi[16] R.Raghavan[8] G.Rahal-Callot[44] P.G.Rancoita[24] M.Rattaggi[24] G.Raven[2] P.Razis[27] K.Read[29] D.Ren[44] Z.Ren[16] M.Rescigno[34] S.Reucroft[10] A.Ricker[1] S.Riemann[43] W.Riemers[41] O.Rind[3] H.A.Rizvi[16] F.J.Rodriguez[23] B.P.Roe[3] M.Röhner[1] S.Röhner[1] L.Romero[23] J.Rose[1] S.Rosier-Lees[4] R.Rosmalen[28] Ph.Rosselet[19] A.Rubbia[13] J.A.Rubio[15] H.Rykaczewski[44] M.Sachwitz[43] E.Sajan[31] J.Salicio[15] J.M.Salicio[23] G.S.Sanders[21] A.Santocchia[31] M.S.Sarakinos[13] G.Sartorelli[7,16] M.Sassowsky[1] G.Sauvage[4] V.Schegelsky[35] K.Schmiemann[1] D.Schmitz[1] P.Schmitz[1] M.Schneegans[4] H.Schopper[45] D.J.Schotanus[28] S.Shotkin[13] H.J.Schreiber[43] J.Shukla[32] R.Schulte[1] S.Schulte[1] K.Schultze[1] J.Schütte[12] J.Schwenke[1] G.Schwering[1] C.Sciacca[26] I.Scott[12] R.Sehgal[16] P.G.Seiler[42] J.C.Sens[15,2] L.Servoli[31] I.Sheer[36] D.Z.Shen[38] S.Shevchenko[30] X.R.Shi[30] E.Shumilov[25] V.Shoutko[25] E.Soderstrom[33] D.Son[46] A.Sopczak[36] C.Spartiotis[5] T.Spickermann[1] P.Spillantini[14] R.Starosta[1] M.Steuer[7,13] D.P.Stickland[33] F.Sticozzi[13] H.Stone[17] K.Strauch[12] B.C.Stringfellow[41] K.Sudhakar[8,1] G.Sultanov[16] R.L.Sumner[33] L.Z.Sun[18,16] H.Suter[44] R.B.Sutton[32] J.D.Swain[16] A.A.Syed[16] X.W.Tang[6] L.Taylor[10] G.Terzi[24] C.Timmermans[28] Samuel C.C.Ting[13] S.M.Ting[13] M.Tonutti[1] S.C.Tonwar[8] J.Tóth[11] A.Tsaregorodtsev[35] G.Tsipolitis[32] C.Tully[30] K.L.Tung[6] J.Ulbricht[44] L.Urbán[11] U.Uwer[1] E.Valente[34] R.T.Van de Walle[28] I.Vetlitsky[25] G.Viertel[44] P.Vikas[16] U.Vikas[16] M.Vivargent[4] H.Vogel[32] H.Vogt[43] I.Vorobiev[25] A.A.Vorobyov[35] L.Vuilleumier[19] M.Wadhwa[16] W.Wallraff[1] C.R.Wang[18] G.H.Wang[32] J.H.Wang[6] Q.F.Wang[12] X.L.Wang[18] Y.F.Wang[13] Z.M.Wang[16,18] A.Weber[1] J.Weber[44] R.Weill[19] T.J.Wenaus[20] J.Wenninger[17] M.White[13] C.Willmott[23] F.Wittgenstein[15] D.Wright[33] R.J.Wu[6] S.X.Wu[16] Y.G.Wu[6] B.Wysłouch[13] Y.Y.Xie[38] Y.D.Xu[6] Z.Z.Xu[18] Z.L.Xue[38] D.S.Yan[38] X.J.Yan[13] B.Z.Yang[18] C.G.Yang[6] G.Yang[16] K.S.Yang[6] Q.Y.Yang[6] Z.Q.Yang[38] C.H.Ye[16] J.B.Ye[18] Q.Ye[16] S.C.Yeh[47] Z.W.Yin[38] J.M.You[16] N.Yunus[16] M.Yzerman[2] C.Zaccardelli[30] P.Zemp[44] M.Zeng[16] Y.Zeng[1] D.H.Zhang[2] Z.P.Zhang[18,16] B.Zhou[9] J.F.Zhou[1]

R.Y.Zhu,[30] H.L.Zhuang,[6] A.Zichichi,[7,15,16] B.C.C.van der Zwaan.[2]

 1 I. Physikalisches Institut, RWTH, W-5100 Aachen, FRG[§]

    III. Physikalisches Institut, RWTH, W-5100 Aachen, FRG[§]

 2 National Institute for High Energy Physics, NIKHEF, NL-1009 DB Amsterdam, The Netherlands

 3 University of Michigan, Ann Arbor, MI 48109, USA

 4 Laboratoire d'Annecy-le-Vieux de Physique des Particules, LAPP,IN2P3-CNRS, BP 110, F-74941
    Annecy-le-Vieux CEDEX, France

 5 Johns Hopkins University, Baltimore, MD 21218, USA

 6 Institute of High Energy Physics, IHEP, Beijing, P.R. China

 7 INFN-Sezione di Bologna, I-40126 Bologna, Italy

 8 Tata Institute of Fundamental Research, Bombay 400 005, India

 9 Boston University, Boston, MA 02215, USA

10 Northeastern University, Boston, MA 02115, USA

11 Central Research Institute for Physics of the Hungarian Academy of Sciences, H-1525 Budapest 114, Hungary

12 Harvard University, Cambridge, MA 02139, USA

13 Massachusetts Institute of Technology, Cambridge, MA 02139, USA

14 INFN Sezione di Firenze and University of Florence, I-50125 Florence, Italy

15 European Laboratory for Particle Physics, CERN, CH-1211 Geneva 23, Switzerland

16 World Laboratory, FBLJA Project, CH-1211 Geneva 23, Switzerland

17 University of Geneva, CH-1211 Geneva 4, Switzerland

18 Chinese University of Science and Technology, USTC, Hefei, Anhui 230 029, P.R. China

19 University of Lausanne, CH-1015 Lausanne, Switzerland

20 Lawrence Livermore National Laboratory, Livermore, CA 94550, USA

21 Los Alamos National Laboratory, Los Alamos, NM 87544, USA

22 Institut de Physique Nucléaire de Lyon, IN2P3-CNRS,Université Claude Bernard, F-69622 Villeurbanne Cedex,
    France

23 Centro de Investigaciones Energeticas, Medioambientales y Tecnologicas, CIEMAT, E-28040 Madrid, Spain

24 INFN-Sezione di Milano, I-20133 Milan, Italy

25 Institute of Theoretical and Experimental Physics, ITEP, Moscow, Russia

26 INFN-Sezione di Napoli and University of Naples, I-80125 Naples, Italy

27 Department of Natural Sciences, University of Cyprus, Nicosia, Cyprus

28 University of Nymegen and NIKHEF, NL-6525 ED Nymegen, The Netherlands

29 Oak Ridge National Laboratory, Oak Ridge, TN 37831, USA

30 California Institute of Technology, Pasadena, CA 91125, USA

31 INFN-Sezione di Perugia and Universitá Degli Studi di Perugia, I-06100 Perugia, Italy

32 Carnegie Mellon University, Pittsburgh, PA 15213, USA

33 Princeton University, Princeton, NJ 08544, USA

34 INFN-Sezione di Roma and University of Rome, "La Sapienza", I-00185 Rome, Italy

35 Nuclear Physics Institute, St. Petersburg, Russia

36 University of California, San Diego, CA 92182, USA

37 Dept. de Fisica de Particulas Elementales, Univ. de Santiago, E-15706 Santiago de Compostela, Spain

38 Shanghai Institute of Ceramics, SIC, Shanghai, P.R. China

39 Bulgarian Academy of Sciences, Institute of Mechatronics, BU-1113 Sofia, Bulgaria

40 University of Alabama, Tuscaloosa, AL 35486, USA

41 Purdue University, West Lafayette, IN 47907, USA

42 Paul Scherrer Institut, PSI, CH-5232 Villigen, Switzerland

43 DESY-Institut für Hochenergiephysik, O-1615 Zeuthen, FRG

44 Eidgenössische Technische Hochschule, ETH Zürich, CH-8093 Zürich, Switzerland

45 University of Hamburg, W-2000 Hamburg, FRG

46 Center for High Energy Physics, South Korea

47 High Energy Physics Group, Taiwan, ROC

 § Supported by the German Bundesministerium für Forschung und Technologie

 † Deceased.

References

[1] S. Jadach, Z. Was *et al.* in "Z Physics at LEP1", CERN Report CERN-89-08, eds G. Altarelli, R. Kleiss and C. Verzegnassi (CERN, Geneva, 1989) Vol. 1, p. 235.

[2] S.L. Glashow, *Nucl. Phys.* **22** (1961) 579;
S. Weinberg, *Phys. Rev. Lett.* **19** (1967) 1264;
A. Salam, Elementary Particle Theory, Ed. N. Svartholm, Stockholm, "Almquist and Wiksell" (1968), 367.

[3] Y. S. Tsai, *Phys. Rev.* **D4** (1971) 2821.

[4] ARGUS Collaboration, H. Albrecht *et al.*, *Phys. Lett.* **B246** (1990) 278.

[5] ARGUS Collaboration, H. Albrecht *et al.*, *Phys. Lett.* **B250** (1990) 164.

[6] K. Hagiwara, A. D. Martin, D. Zeppenfeld, *Phys. Lett.* **B235** (1990) 198;
A. Rougé, Z. Phys. **C48** (1990) 75.

[7] L3 Collaboration, B. Adeva *et al.*, *Z. Phys.* **C51** (1991), 179;
L3 Collaboration, B. Adeva *et al.*, "Measurement of $e^+e^- \rightarrow b\bar{b}$ and $e^+e^- \rightarrow c\bar{c}$ Forward-Backward Asymmetry at the Z^0 Resonance", CERN-PPE/92-121, July 1992, submitted to *Phys. Lett.*

[8] L3 Collaboration, B. Adeva *et al.*, *Nucl. Instr. and Meth.* **A289** (1990) 35.

[9] O. Adriani *et al.*, *Nucl. Instr. and Meth.* **A302** (1991) 53;
K. Deiters et al., DESY-PHE 91-015, December 1991, submitted to *Nucl. Inst. and Meth.*

[10] J. A. Bakken, *Nucl. Instr. and Meth.* **A275** (1989) 81.

[11] T. Sjöstrand and M. Bengtsson, *Comput. Phys. Commun.* **43** (1987) 367;
T. Sjöstrand in "Z Physics at LEP1", CERN Report CERN-89-08, Vol. 3, p. 143.

[12] S. Jadach and Z. Was, *Comput. Phys. Commun.* **35** (1985);
R. Kleiss, "Z Physics at LEP", CERN-8908 (1989), Vol. III, p. 1.

[13] The L3 detector simulation is based on GEANT Version 3.14.
See R. Brun *et al.*, "GEANT 3", CERN DD/EE/84-1 (Revised), September 1987.
The GHEISHA program (H. Fesefeldt, RWTH Aachen Preprint PITHA 85/02 (1985)) is used to simulate hadronic interactions.

[14] K. Hikasa *et al.*, Review of Particle Properties, *Phys. Rev.* **D45**, No. 11, (1992).

[15] M. G. Bowler, *Phys. Lett.* **B182** (1986) 400;
M. Feindt, *Z. Phys.* **C48** (1990) 681;
J. H. Kühn and A. Santamaria, *Z. Phys.* **C48** (1990) 445;
L. M. Barkov, *et al.*, *Nucl. Phys.* **B256** (1985) 365.

[16] A. Rougé, Workshop on Tau Lepton Physics, Orsay, 24-27 September, 1990;
A. Rougé, *Z. Phys.* **C48** (1990) 75;

[17] A. Walther, Dissertation, Universität Dortmund, 1991, *Untersuchung des Zerfalls* $\tau^- \to \pi^-\pi^-\pi^+\nu_\tau$ *und Bestimmung der Helizität des Tauneutrinos.*

[18] V.Innocente, Y.F.Wang and Z.P.Zhang, CERN-PPE/92-98, submitted to *Nucl. Inst. and Meth.*

[19] Aleph Collaboration, D. Decamp *et. al.*, Phys. Lett. **B265** (1991) 430;
Opal Collaboration, G. Alexander *et. al.*, Phys. Lett. **B266** (1991) 201;
Delphi Collaboration, CERN Preprint, CERN-PPE/92-60, (1992).

[20] C. Prescott *et al.*, *Phys. Lett.* **84B** (1979), 524.

[21] M. Consoli, W. Hollik and F. Jegerlehner, in "Z Physics at LEP1", CERN Report CERN 89-08, eds G. Altarelli,R. Kleiss and C. Verzegnassi (CERN, Geneva, 1989) Vol.1,p.7.
S. N. Ganguli, CERN/PRE/91-081, October 1991.
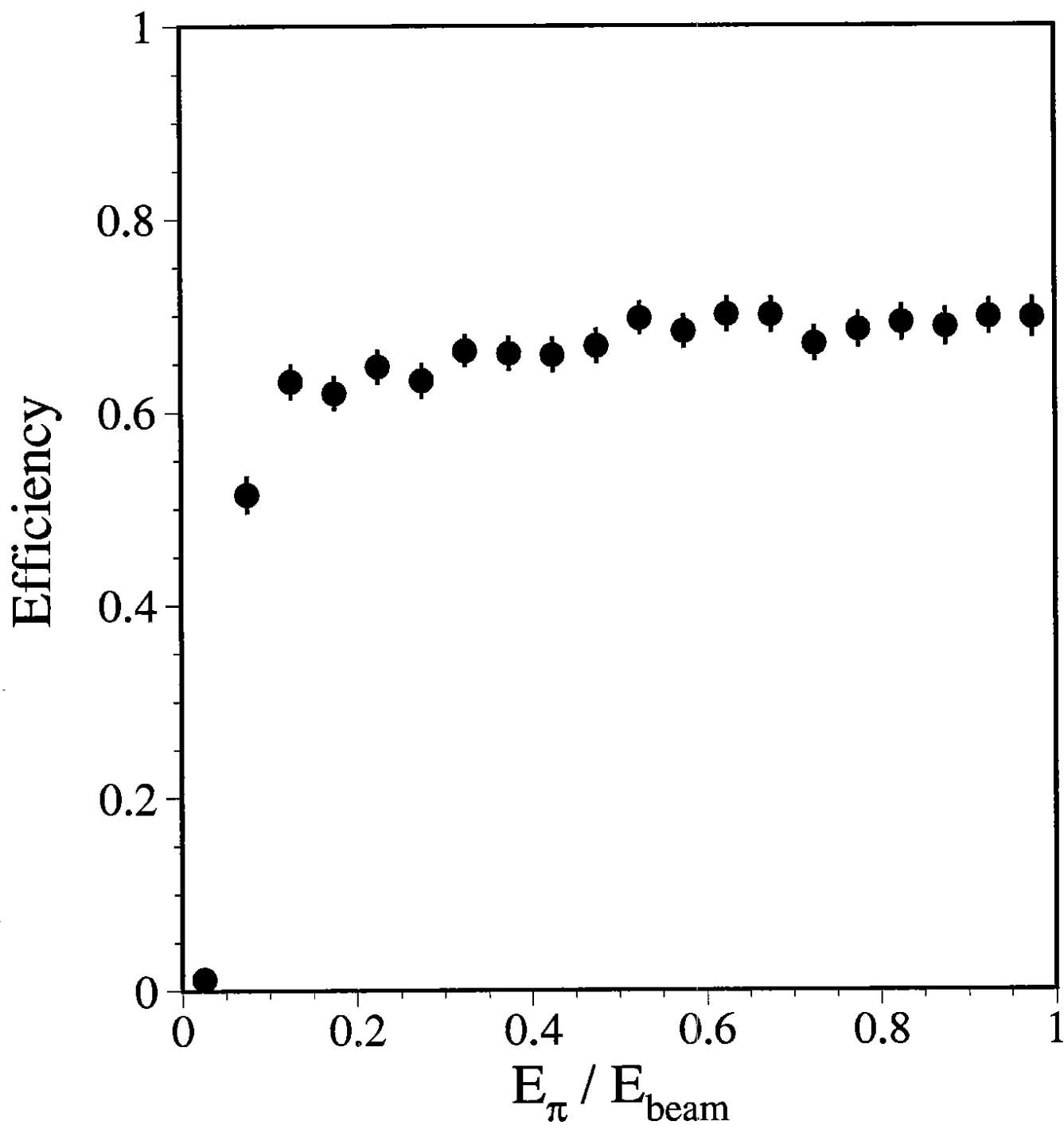
Figure 1: Selection efficiency of $\tau^- \to \pi^-(K^-)\nu_\tau$ decays as a function of $x_\pi = E_\pi/E_{\text{beam}}$ for 1991 data.
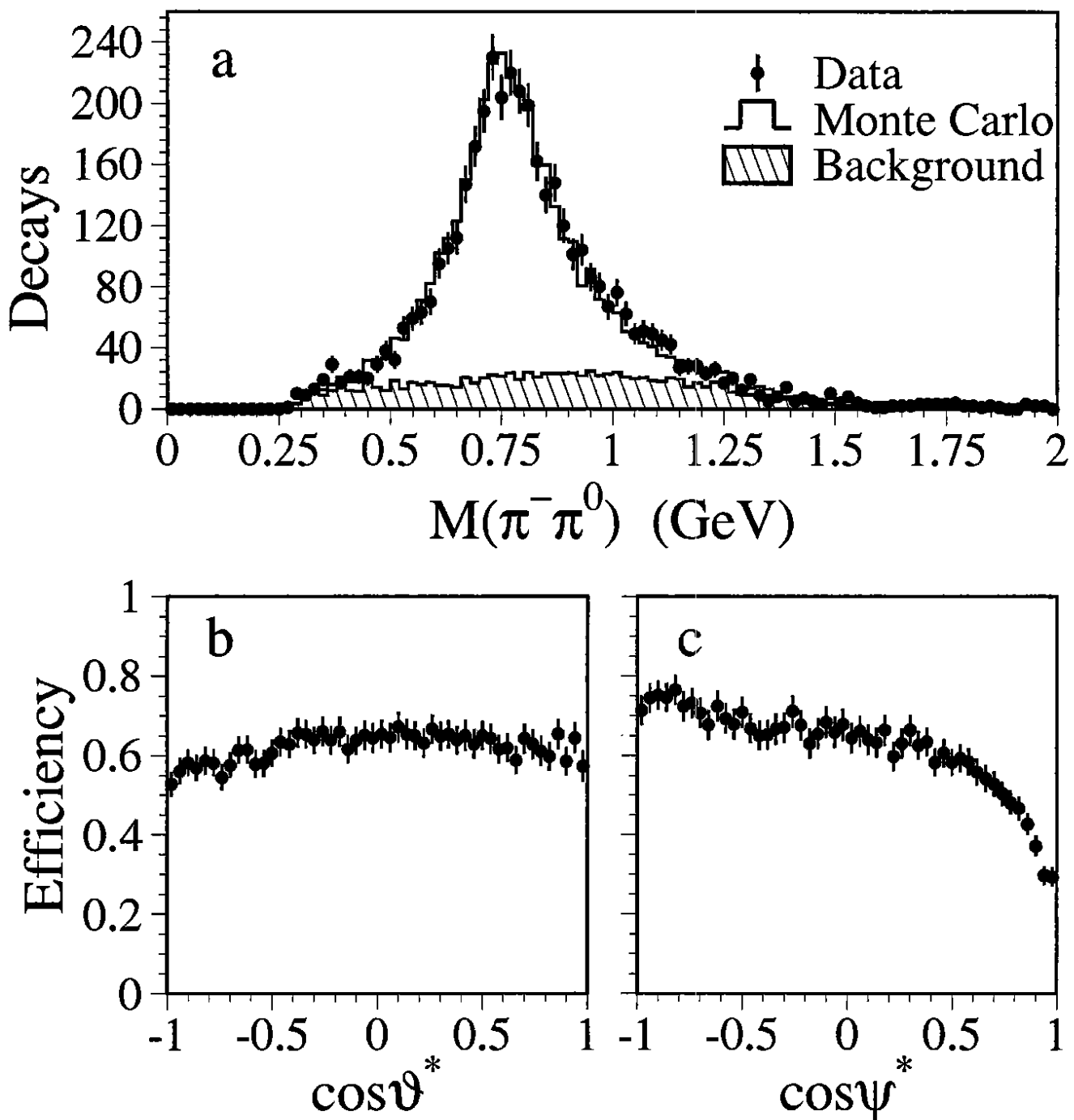
Figure 2: a)The invariant mass of the $\pi^{\pm}\pi^0$ for selected $\tau^- \to \rho^-\nu_\tau$ candidates compared with Monte Carlo prediction. b) The efficiency for $\tau^- \to \rho^-\nu_\tau$ decays as a function of $\cos\theta^*$ for 1991 data. c) The efficiency of $\tau^- \to \rho^-\nu_\tau$ decays as a function of $\cos 42^*$ for 1991 data. The fall off near $\cos 42^* = 1$ corresponds to the kinematic region where the $\pi^{\pm}$ carries most of the $\rho^{\pm}$ energy and whose showers in the BGO calorimeter are merged with the those of the π^0.
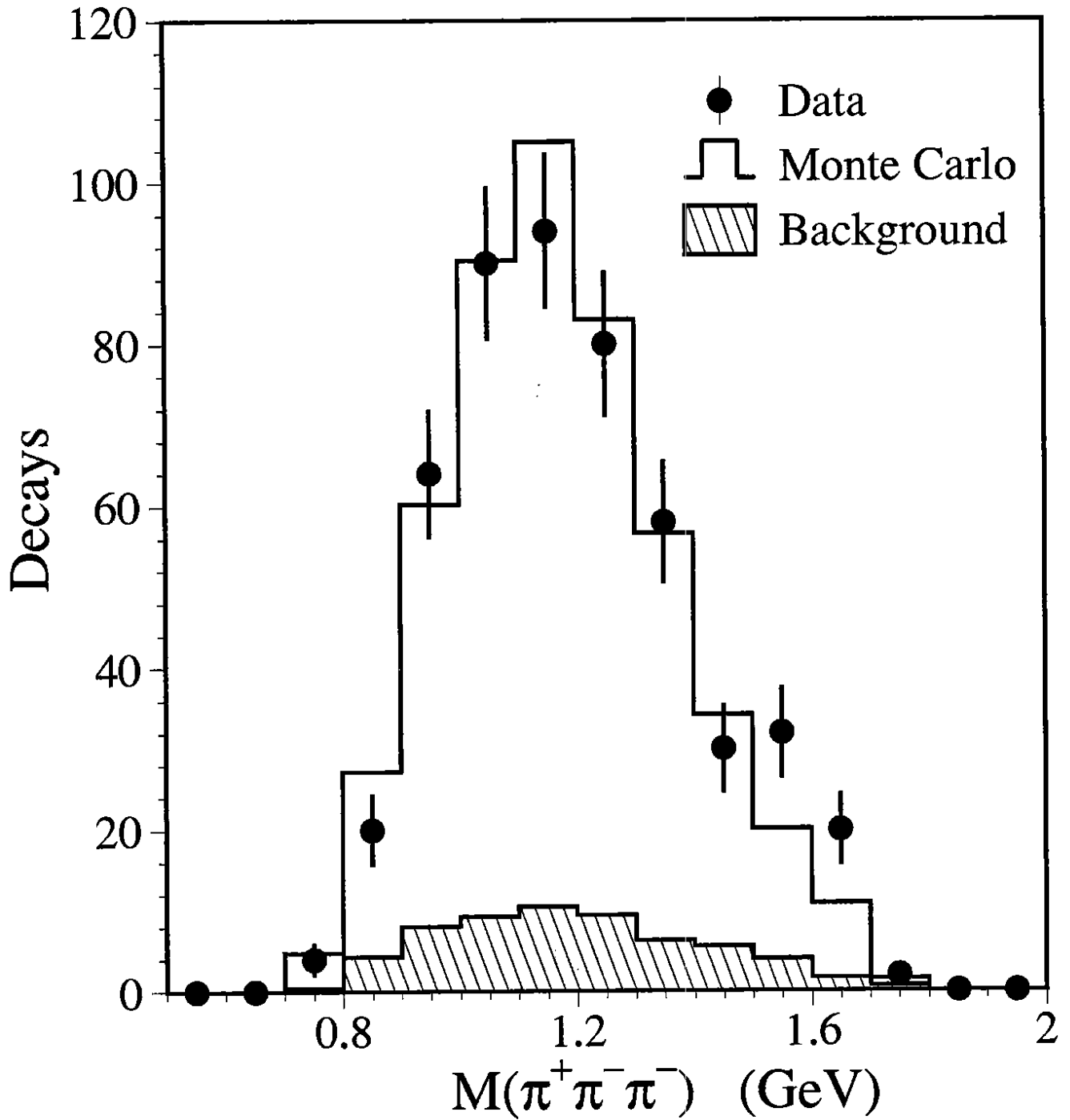
Figure 3: Invariant mass distribution of $\tau^- \to \pi^-\pi^+\pi^-\nu_\tau$ compared with Monte Carlo.
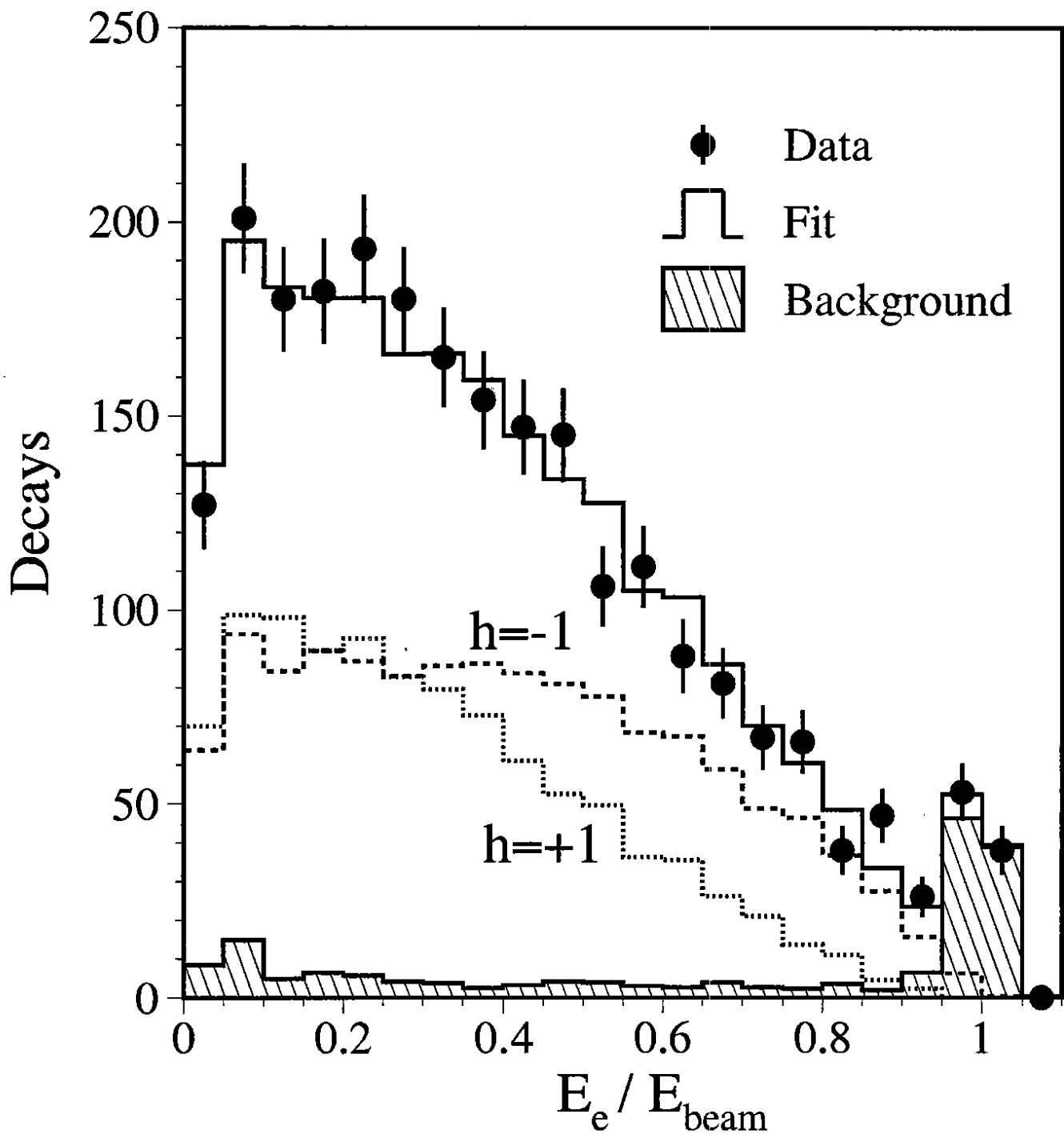
Figure 4: The spectrum of $\tau^- \to e^- \bar{\nu}_e \nu_\tau$ decays as a function of $x_e = E_e/E_{\text{beam}}$. Also shown is the contribution from each helicity including backgrounds for that helicity. The hatched histogram shows the total background.
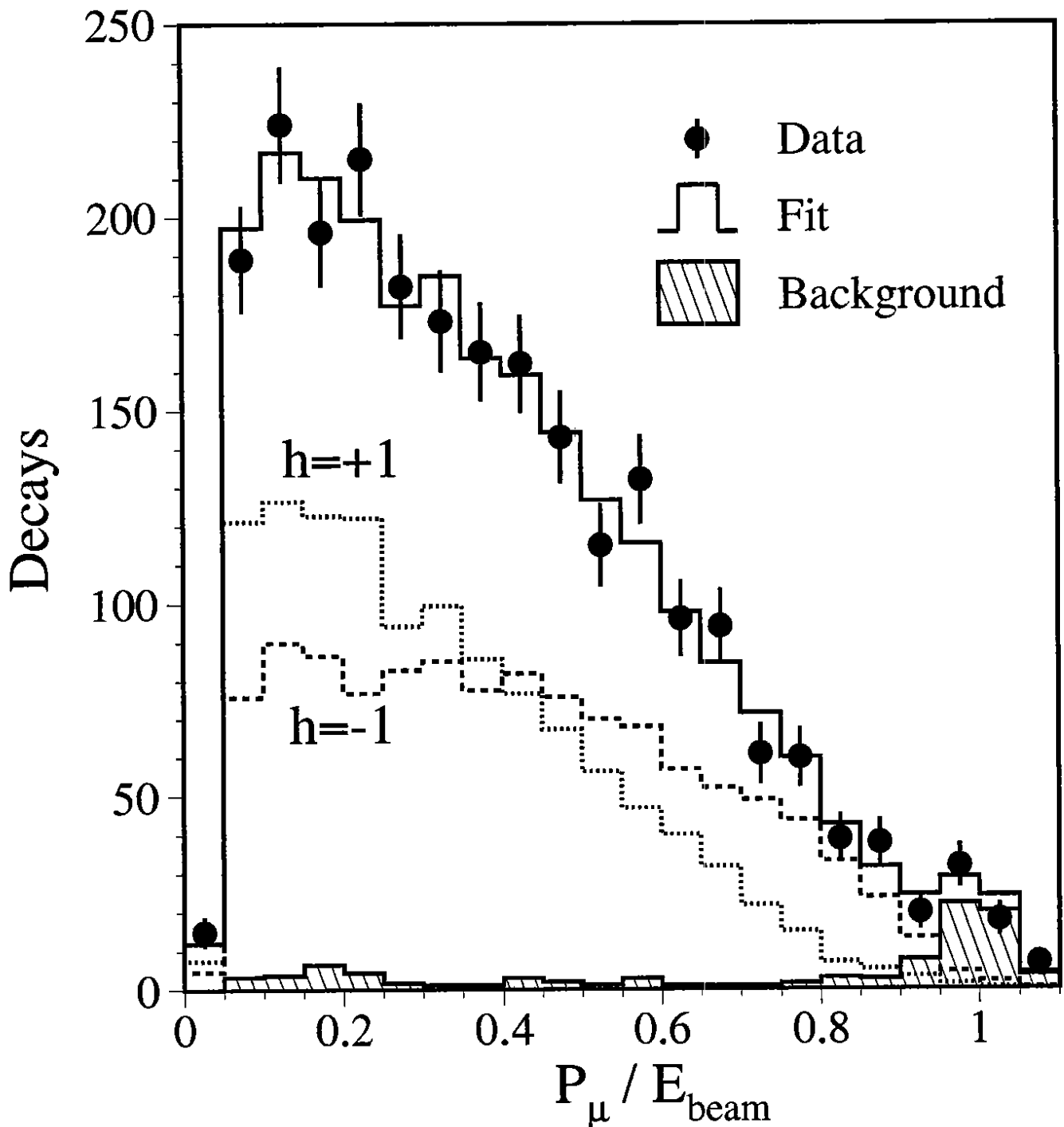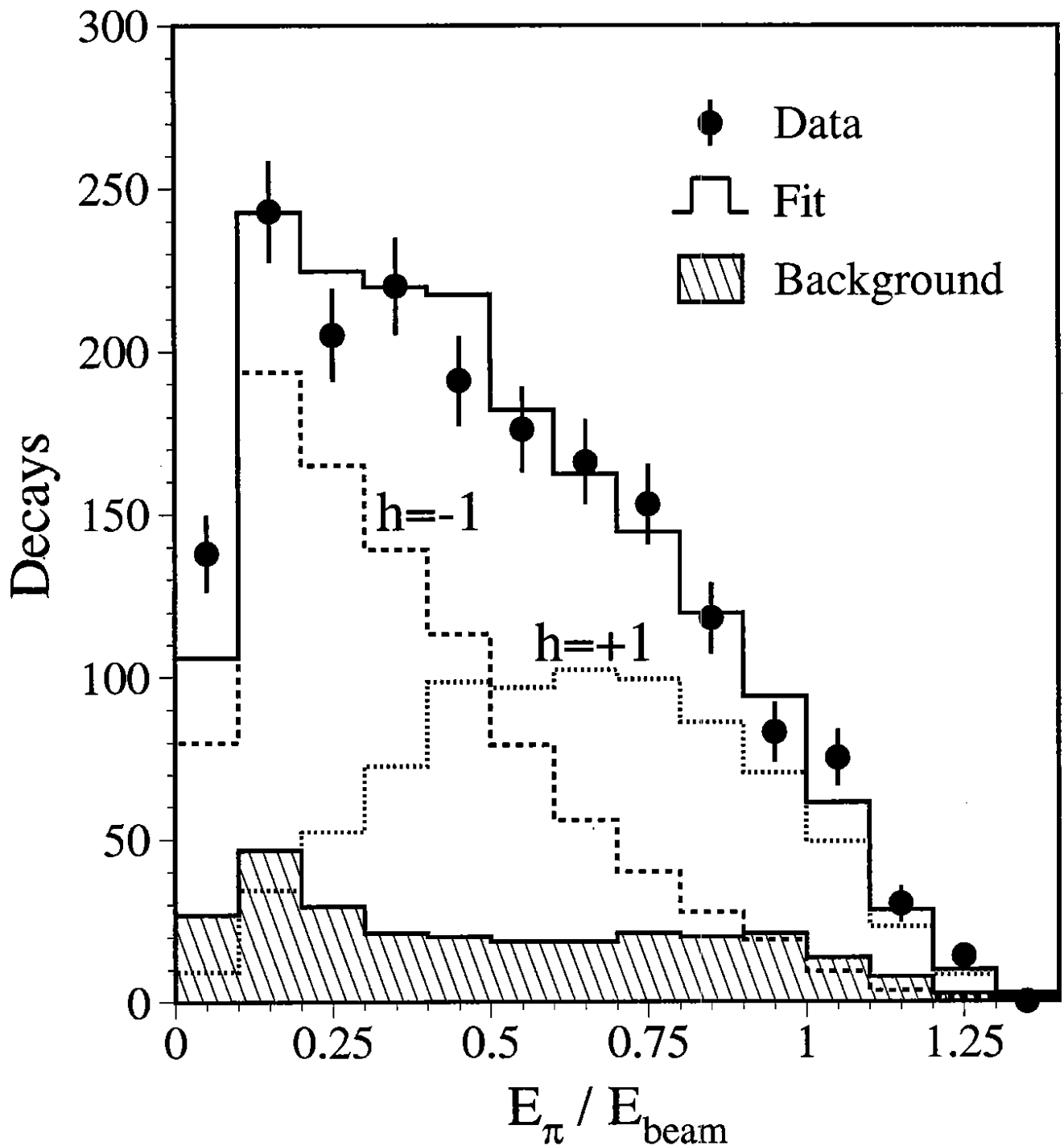
Figure 5: The spectrum of $\tau^- \to \mu^- \overline{\nu}_\mu \nu_\tau$ decays as a function of $x_\mu = E_\mu / E_{\text{beam}}$. Also shown is the contribution from each helicity including backgrounds for that helicity. The hatched histogram shows the total background.

Figure 6: The spectrum of $\tau^- \to \pi^-(K^-)\nu_\tau$ decays as a function of $x_\pi = E_\pi/E_{\text{beam}}$. Also shown is the contribution from each helicity including backgrounds for that helicity. The hatched histogram shows the total background.
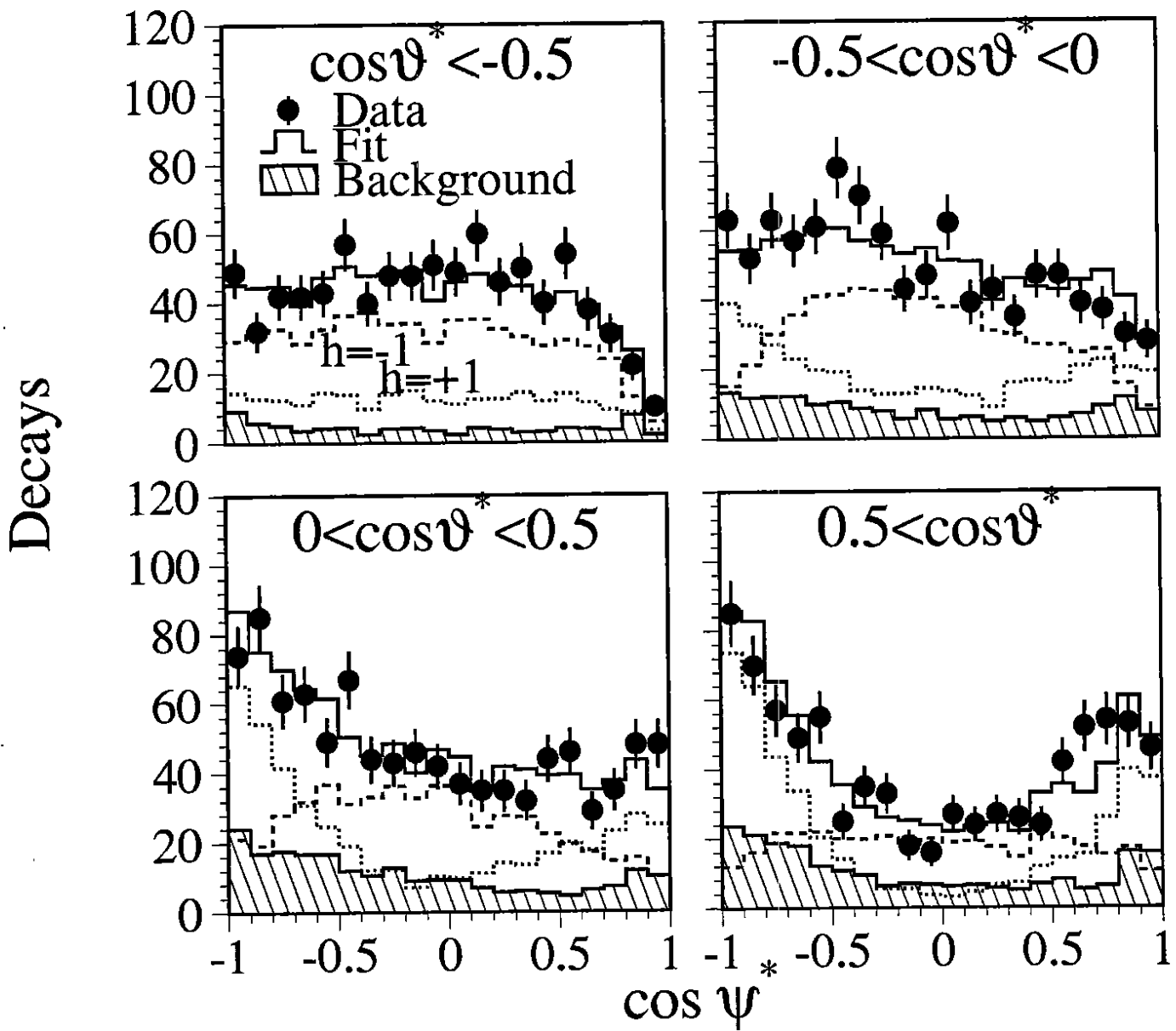
Figure 7: The spectra of $\tau^- \to \rho^- \nu_\tau$ decays as a function of cos 42^* for four ranges of cos θ^* (See text for definitions). Also shown is the contribution from each helicity including backgrounds for that helicity. The hatched histogram shows the total background.